Chemical Engineering Journal 426 (2021) 131269

Contents lists available at ScienceDirect

Chemical Engineering Journal

journal homepage: www.elsevier.com/locate/cej

Sulfonated polyaniline assisted hierarchical assembly of graphene-LDH nanohybrid for enhanced anticorrosion performance of waterborne epoxy coatings

Yue Su [a,b,c], Shihui Qiu [a,b], Jiayu Wei [a], Xiaobo Zhu [a,b], Haichao Zhao [a,*], Qunji Xue [a,*]

[a] Key Laboratory of Marine Materials and Related Technologies, Zhejiang Key Laboratory of Marine Materials and Protective Technologies, Ning–bo Institute of Materials Technology and Engineering, Chinese Academy of Sciences, Ningbo 315201, China
[b] University of Chinese Academy of Sciences, Beijing 100049, China
[c] Innovation Academy of South China Sea Ecology and Environmental Engineering, Chinese Academy of Sciences, Guangzhou 510301, China

ARTICLE INFO

Keywords:
Graphene
Insulation package
Good compatibility
Epoxy coating
Anticorrosion

ABSTRACT

The strong barrier of well dispersed graphene provides excellent labyrinth effect in organic coating. However, the high conductive graphene sheets are prone to forming conductive path in coating matrix with corrosive medium, resulting in serious micro current corrosion. Although a large number of methods to reduce the conductivity of graphene have been reported, how to balance the conductivity of graphene, the affinity between filler and resin, and the self-healing property of coating are major issues for researchers to consider. Here, we have developed a strategy for insulating graphene with layered double hydroxides via sulfonated polyaniline mediated self-assembly approach. Graphene sheets were stripped by sulfonated polyaniline to improve the interlayer spacing of graphene followed by covered with layered double metal hydroxide (LDH) via ionic crosslinking, which reduced the conductivity of graphene and improve the interfacial compatibility between the fillers and the resin. At the same time, the electroactive polyanilines between the graphene layers afford the coating with self-healing effect. The novel graphene-LDH nanohybrid material was incorporated into the waterborne epoxy resin to prepare corrosion resistant coatings with a thickness of about 70 ± 5 μm. The electrochemical and self-healing properties of the prepared composite coating were characterized by EIS, Tafel and LEIS techniques. This novel sulfonated polyaniline crosslinked graphene-LDH nanohybrid expands in the research and development of graphene based high performance anticorrosive coatings.

1. Introduction

Graphene exhibits outstanding impermeability, large specific surface areas and high aspect ratios, which can be the ideal physical barrier [1–4]. When added to the organic resin, graphene can remedy the micro-pores at lower loading capacity and improve the barrier property of organic coatings [5–8]. However, there are two disadvantages of graphene used for anticorrosion, one is the case of agglomeration that could introduce the defects and free volumes in the coating, the other is the acceleration of corrosion caused by high conductivity of graphene sheets [9–11].

In order to address these issues, researchers have made use of the π-π* interactions between graphene and electroactive substances including polycyclic aromatic hydrocarbons (such as pyrene [12–14], naphthalene [15], anthracene [16], tetracene [17], coronene [18] and ovalene[19]) and conductive polymers (such as polyaniline [7,20–22], polypyrrole [5,23], polythiophene [24], polydopamine [25] and so on) to achieve the exfoliation of graphene sheets and enhance the chemical compatibility with coating matrix, conductive polymers also contribute to the formation of passivation oxides layers on the steel surface to decrease the local electrochemical activity of the steel.

The above methods mainly solve the problem of graphene agglomeration, while it also couldn't be omitted that graphene possesses high conductivity, which can accelerate charges transfer and form graphene-metal micro-galvanic cell corrosion at the coating defects [26]. In order to reduce the conductivity of graphene, nanoscale SiO_2 was used to encapsulate reduced graphene oxide (rGO), the nanoscale SiO_2 grown on the surface of graphene could prevent graphene from contacting metal [27]. This measure could effectively eliminate graphene-metal

* Corresponding authors.
E-mail addresses: zhaohaichao@nimte.ac.cn (H. Zhao), qjxue@nimte.ac.cn (Q. Xue).

https://doi.org/10.1016/j.cej.2021.131269
Received 3 December 2020; Received in revised form 6 May 2021; Accepted 8 July 2021
Available online 14 July 2021

micro-galvanic cell corrosion. In addition to the in-situ synthesis of inorganic nanoparticles, organic insulative polymers (such as pernigraniline [28], (3-aminopropyl)-triethoxysilane (APTES) [29]) could also attach to the surface of graphene or graphene oxides to cut down the conductivity of graphene. The presence of these organic polymers could effectively encapsulate graphene and avoid direct contact between graphene and metal interface. Furthermore, furan epoxide was selected as the insulating packaging material to prepare furan-graphene composites by the Diels-Alder reaction [30]. The prepared composites decreased the electrical conductivity and exhibited outstanding compatibility with polymer.

Meanwhile, the conductivity of graphene can also be decreased by elements doped method. Fluorinated graphene was prepared by liquid phase stripping successfully, which was significantly lowering the conductivity of graphene [31]. In order to reveal the mechanism of different elements, B-doped and N-doped graphene by thermal stripping of graphene oxide were obtained [32]. There are significant differences in electronic properties of doped materials. Results show that B atom acts as an electron acceptor reduces the conductivity of graphene, but the doped of electron donor N improves the conductivity of graphene [32–33]. However, the element doped method is complicated in operation and not suitable for large-scale production.

Layered double hydroxide (LDH) is a kind of insulating two-dimensional nanomaterial, which is composed of positively charged main laminates, the interlayer anions and water molecules overlap each other. In order to achieve the exfoliation of graphene and the reduction of conductivity, we designed a sandwich structure of graphene-LDH hybrids using sulfonated polyaniline (SPANI) as noncovalent dispersing agent and ionic interacting agent for LDH as shown Fig. 1. First, thin layers of graphene with large amounts of negative charges on the surface were generated by the π-π* interaction between SPANI and graphene sheets. LDH sheets were then assembled on the surface of graphene surface by ionic crosslinking of SPANI and LDH. This preparation process was simple and did not destroy the original structure of graphene. Further, the surface adsorbed LDH contained a large amount of hydroxyl groups, which improved the solubility of the composite nanomaterial in the resin and prevented graphene from interconnecting to form a conductive path. The structure and morphology of G-SPANI-LDH composites were characterized by Raman, XRD, XPS, SEM, TEM. Whereafter, the nanocomposites were dispersed in a resin to prepare anticorrosive coatings, with the thicknesses of the coatings about 70 ± 5 μm. The self-healing and anticorrosive properties of as prepared coatings were investigated by LEIS, EIS, potentiodynamic polarization curves and salt spray test.

2. Experiment part

2.1. Materials

Graphene was bought from Ashine New Carbon Material Co., Ltd. Magnesium nitrate hexahydrate, aluminum nitrate nonahydrate, urea, sodium chloride, aniline, 2-aminobenzenesulfonic acid, sodium persulfate and polyether amine D230 were purchased from Aladdin Reagent Co. Ltd., all of them were directly used without further purification. Waterborne epoxy was purchased from Shenyang Baichen Chemical Technology Co. Ltd. The Q235 mild steel (contact area of 1 cm^2) electrodes were acquired from Shengxin Technology Co., Ltd. The carbon steel with an area of 1 cm × 1 cm was polished with 400 and 800C sandpapers and cleaned in ethanol and acetone by ultrasonic vibration.

2.2. Material synthesis and coating preparation

2.2.1. Synthesis of sulfonated polyaniline

Sulfonated polyaniline (SPANI) was obtained by the following steps. Firstly, 4.3 g of aniline and 2.3 g of 2-aminobenzenesulfonic acid were completely dissolved in 500 mL of 1 M HCl aqueous solution. 500 mL of 1 M HCl solution with 11.4 g $(NH_4)_2S_2O_8$ were added into the above prepared mixed solution. Subsequently, the reaction was carried out at 0 °C for 24 h without interference. The green and black products were collected by filtration, washed repeatedly with deionized water, and finally dried in a vacuum oven at 60 °C for 12 h.

2.2.2. Synthesis of LDH

2 mmol of $Mg(NO_3)_2{\cdot}6H_2O$, 1 mmol of $Al(NO_3)_3{\cdot}9H_2O$ and 7 mmol of $CO(NH_2)_2$ were dissolved in 70 mL of deionized water and taken to react in a tetrafluoroethylene reactor at 140 °C for 8 h. After the reaction, the obtained product was centrifuged, washed and dried in an oven at 60 °C for 12 h.

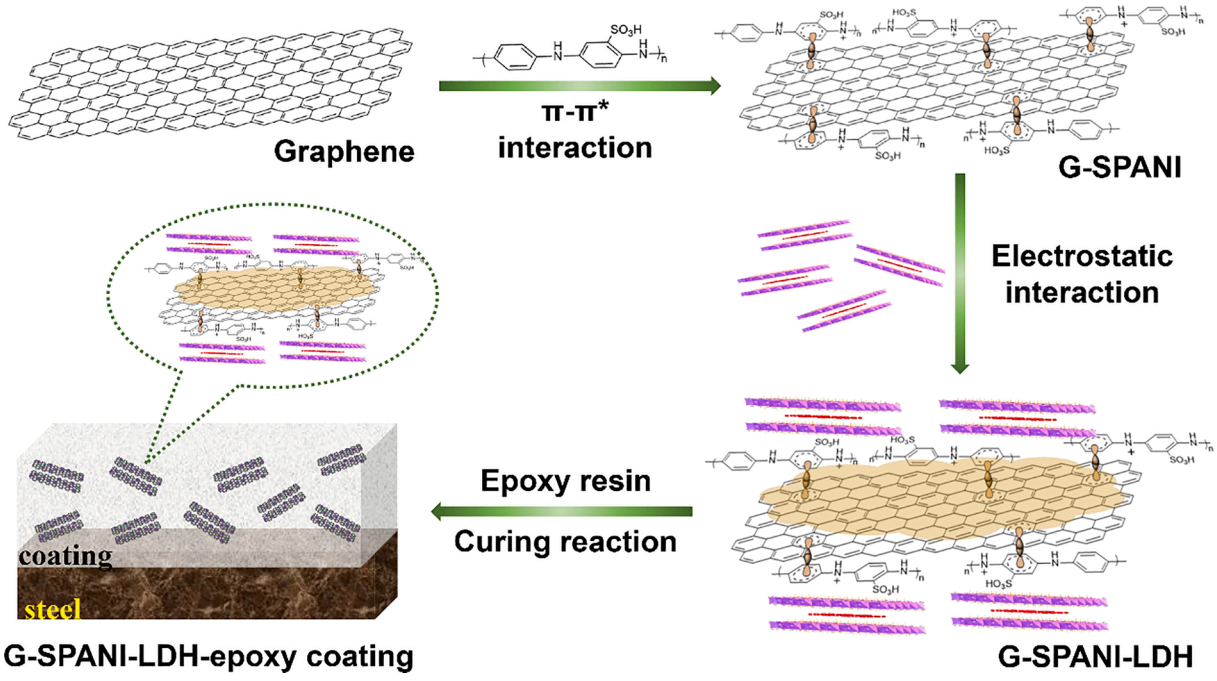

Fig. 1. Schematic preparation of graphene-LDH nanohybrid via sulfonated polyaniline mediated self-assembly approach and G-SPANI-LDH epoxy coating.

2.2.3. Synthesis of G-SPANI-LDH

A certain amount of graphene and sulfonated polyaniline (with a mass ration of 1:2) were dissolved in 100 mL of deionized water under ultrasonic irradiation of 60 W for 20 mins, and LDH was dispersed in the above solution (m_{LDH}:m_G = 5:1) and stirred for 2 h at 300 rpm (m_G:m_{SPANI}:m_{LDH} = 1:2:5). Afterwards, the hybrids were centrifuged at 6000 rpm, washed, and finally dried at 60 °C for 12 h. Graphene is easy to agglomerate, sulfonated polyaniline is used to peel graphene to improve the interlayer spacing of graphene. After graphene was stripped by SPANI, LDH was coated on the surface of G-SPANI to prepare G-SPANI-LDH.

2.2.4. Preparation of coatings

The prepared G and G-SPANI-LDH were weighed (0.5 wt% per sample) and dissolved in 1 mL of ethanol. In order to obtain uniform dispersion, ultrasonic treatment was performed for 5 mins. Then, 1 g of polyether amine D230 was added to the above mixed solution and stirred violently for 20 mins. After that, 5 g of waterborne epoxy resin was mixed into the above mixture and stirred for 10 mins. Before using, the residual ethanol was evaporated at 60 °C by a rotary evaporator. The resin was coated on the surface of Q235 steel with a wire rod, and the dry film thicknesses were 70 ± 5 μm after curing reaction. Besides, pure epoxy coatings were selected as blank samples (EP). To distinguish the composite coatings, they were represented as pure-epoxy coating, G-epoxy coating and G-SPANI-LDH-epoxy coating.

2.3. Characterization method

2.3.1. Characterization of materials

The chemical structure of G-SPANI-LDH was characterized by Raman spectroscopy (Renishaw invia reflex) from 3000 cm^{-1} to 400 cm^{-1}. The crystal structures of G, G-SPANI and G-SPANI-LDH were characterized by X-ray diffraction (D8 advance, Bruker). The XRD patterns were obtained by using monochromatic Cu Kα radiation in the range of 5-60° at a rate of 3°/min. X-ray photoelectron spectroscopy (XPS, axis ultra, DLD) was used to detect chemical composition and element analysis. The thermal properties of the materials were tested by diamond TG/DTA. The test temperature range was 30–800 °C, and the heating rate was 10 °C/min. The structure and morphology of G-SPANI-LDH were studied by scanning electron microscopy (SEM, Hitachi S4800) and transmission electron microscopy (TEM, TECNAI F20). SEM (Hitachi S4800) and TEM (JEOL 2100) were used to identify the fracture surface morphology and the distribution of coating fillers. The dispersion of fillers was characterized by inVia Raman microscope (Renishaw PLC). The excitation wavelength was 785 nm, the scanning area was 50 μm × 50 μm, and the step size was 1 μm. . The conductivities of the samples were obtained by measuring five different positions using four-probe conductivity meter (CRESBOX). The sample powders were pressed into thin plates with radius of 0.5 cm × 0.5 cm and thicknesses of 1mm.

2.3.2. Electrochemical performance test

CHI-660E electrochemical workstation was used to evaluate the long-term corrosion behavior of coatings in 3.5 wt% NaCl solution. In this experiment, saturated calomel electrode (SCE) and platinum plate were used as reference electrode and counter electrode, respectively. The EIS (electrochemical impedance spectroscopy) data of the prepared samples were carried out in the frequency range of 10^5 Hz to 10^{-2} Hz with sinusoidal disturbance of 20 mV amplitude. The potentiodynamic polarization curves were obtained from cathode to anode (E_{OCP} ± 250 mV) at a scanning rate of 1 mV/s. The thicknesses of samples were 19 ± 1 μm and soaked for 15 days. The EIS results were analyzed by Zview software. The self-healing behavior of the composite coating was detected by LEIS (localized electrochemical impedance spectroscopy), which was carried out on Versa SCAN Micro-Scanning Electrochemical Workshop (AMETEK, USA). During the test, the amplitude was 50 mV and the test frequency was 10 Hz. According to ASTM B117, salt spray test was used to study the failure behavior of the defective coating in extreme environment.

2.3.3. Characterization of corrosion products

SEM (FEI Quanta FEG 250) and energy dispersive spectroscopy (EDS) were used to examine the long-term corrosion samples. The chemical structure of corrosion products was characterized by Raman spectroscopy (Renishaw inVia reflex), and the distribution of corrosion products on the substrate surface was characterized by inVia Raman microscope (Renishaw PLC). The excitation wavelength was 532 nm, the scanning area was 10 μm × 10 μm, and the step size was 0.5 μm.

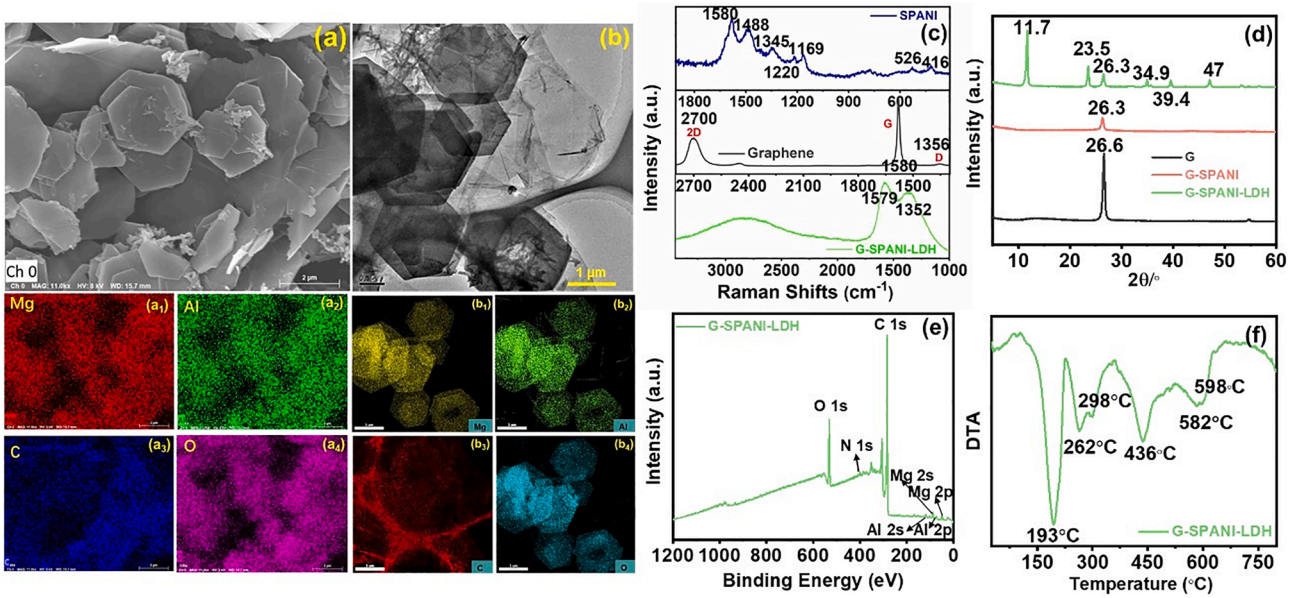

Fig. 2. a, b) The SEM and TEM images of G-SPANI-LDH. a_1-a_4, b_1-b_4) The energy dispersive spectroscopy of G-SPANI-LDH. c) The Raman spectra of SPANI, G and G-SPANI-LDH. d) The XRD patterns of G-SPANI-LDH. e) The XPS full spectrum of G-SPANI-LDH. f) The thermogravimetric curve of G-SPANI-LDH.

Table 1
Conductivity of G and G-SPANI-LDH.

Sample	Conductivity S/cm	Average conductivity S/cm
G	166.7 163.9 163.9 161.3 163.9	163.9 ± 1.7
G-SPANI-LDH	3.0 3.1 2.9 3.0 3.0	3.0 ± 0.1

3. Results and discussion

3.1. Morphology and structure analysis

As displayed in Fig. 1, graphene was stripped by SPANI by π-π* interaction to get G-SPANI nanohybrids. Given the abundant negative charges on the G-SPANI surface, LDH could tightly adsorbed on the surface of G-SPANI through electrostatic interaction after modification to obtain G-SPANI-LDH nanohybrids. The nanohybrid coatings were prepared after the curing reaction.

The morphology of the G-SPANI-LDH composites is shown in Fig. 2a (SEM) and Fig. 2b (TEM) and the element distribution on the surface is shown in Fig. 2a1-2a4 and Fig. 2b1-2b4. As can be seen, LDH is uniformly adsorbed on the graphene surface in hexagonal shape, and the dendritic SPANI is distributed in the middle of graphene and LDH. As shown in Fig. 2c, in Raman spectra, the peaks at 1488 and 1580 cm^{-1} correspond to the benzene and quinone deformation of the SPANI ring [34–36], and the peak at 1345 cm^{-1} is ascribed to the stretching mode of $C\text{-}N^{+}$ radical cation in the protonated state, which proving that SPANI is in the conductive state [37–39]. The peak at 1220 cm^{-1} is assigned to C-N stretching vibration amine type; 1169 cm^{-1} belongs to asymmetric O=S=O stretching vibration peak [40], 416 and 526 cm^{-1} belong to out of plane ring deformation [41]. As shown in Fig. 2c, the D and G peaks of G-SPANI-LDH become wider than that of graphene, which are mainly affected by the SPANI peak.

Graphene was stripped by SPANI. As shown in Fig. 2d XRD pattern, the 2θ peak of graphene appears at 26.6°, and the corresponding layer spacing is 0.33 nm (according to Bragg equation). After graphene is stripped, 2θ moves to 26.3° and the layer spaces increase to 0.34 nm. As displayed in Fig. 2d, there are (003), (006), (012), (015) and (018) peaks in G-SPANI-LDH [42], indicating that LDH distributed on the surface of graphene nanosheets. In order to further explain, we did XPS for element analysis. Fig. 2e shows the full spectrum of G-SPANI-LDH, in which 532 eV belongs to O 1s peak, 400 eV attributes to N 1s peak, 284 eV vests in C 1s peak; 74.5 and 118.5 eV peaks are attributed to Al 2p and Al 2s, while 49.6 and 88.5 eV peaks belong to Mg 2p, Mg 2s [26].

The thermal property of G-SPANI-LDH was analyzed by DTA as shown in Fig. 2f. At the temperature of 100–200 °C, water molecules interacted in LDH are mainly lost; in the temperature range of 200–400 °C, weight loss corresponds to the removal of interlayer hydroxyl and the decomposition of carbonate, 436 °C may be attributed to the fracture of C-S bond on the main chain of SPANI and the carbonization of polymer molecular chain [43–44]. Above 500 °C, LDH completely decomposes and forms bimetallic oxides.

3.2. Test of sample conductivity

As shown in Table 1, the average conductivity of graphene is 163.9 S/cm. After being coated with LDH, the average conductivity of G-SPANI-LDH decreases to 3.0 S/cm, indicating that the conductivity of graphene is significantly reduced after LDH modifications.

3.3. Characterization of coating cross section morphology and filler dispersion

It is well known that the protective and impermeable properties of composite coatings are related to the dispersion of nanofillers in organic resin matrix [45–47]. In order to observe the dispersion of G-SPANI-LDH nanohybrid in the composite coatings, the fracture surfaces of the coatings were characterized by SEM. As displayed in Fig. 3a1-3c2, the surface of pure epoxy resin is smooth, microcracks would expand rapidly without hindrance. However, added nanofillers provide high and low gullies to the coatings, which can hinder the propagation of microcracks. The compatibility between nanofillers and epoxy is significant, the poor compatibility greatly affects the barrier performance of composite coatings. It can be seen from the brittle fracture section of G-epoxy coating that graphene is clustered in the epoxy, which influencing the barrier performance of coating. G-SPANI-LDH nanofillers are evenly distributed in the resin. The ratio of the peak at 1605 cm^{-1} of epoxy resin [48] to 1350 cm^{-1} of graphene represents the density of graphene in epoxy. The color depth of different areas represents the relative content of fillers in the epoxy. It can be seen that the distribution of G-SPANI-LDH in the matrix (Fig. 3e) is more uniform than graphene in Fig. 3d, which is consistent with the transmission electron microscopes in Fig. 3f-3g.

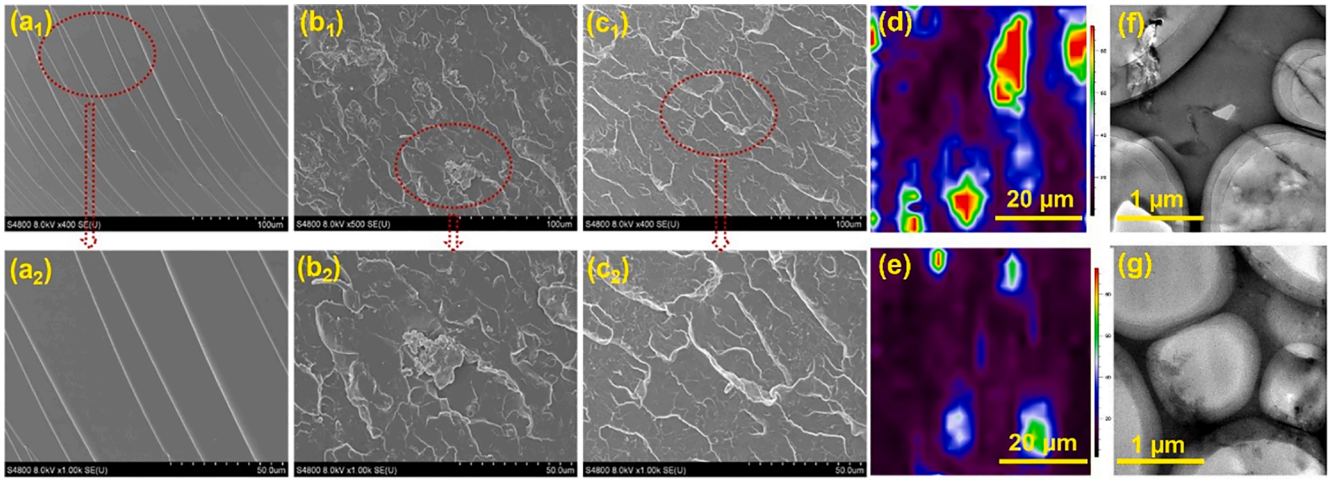

Fig. 3. SEM of brittle fracture interface for a_1, a_2) pure-epoxy coating, b_1, b_2) G-epoxy coating, c_1, c_2) G-SPANI-LDH-epoxy coating. Raman mappings of d) G-epoxy coating and e) G-SPANI-LDH-epoxy coating specimen. The TEM images of f) G-epoxy coating and g) G-SPANI-LDH-epoxy coating.

3.4. Long term corrosion resistance of composites coatings

In order to evaluate the long-term corrosion resistance of nanocomposite coatings in 3.5 wt% NaCl solution, EIS measurements were carried out at different immersion times.

Firstly, the OCP of three coatings was obtained at 1, 10, 30, 50 and 70 days to measure whether it is steady in corrosive environment. OCP can be regarded as the "indicator light" of coating corrosion tendency (Fig. S1, Supporting Information). With the increase of immersion time, the OCP of the pure-epoxy coating decreased rapidly, indicating that corrosive medium can penetrate into the interior of pure-epoxy coating quickly. Added G and G-SPANI-LDH nanofillers can apparently improve the OCP of coatings. However, it was found that the OCP of G-epoxy coating was lower than that of pure-epoxy coating at 30 days, this phenomenon might be ascribed to the agglomeration of graphene. For G-SPANI-LDH-epoxy coating, the good dispersion of graphene could not introduce micropores into epoxy and show a good shielding effect. Even when soaked for 70 days, the OCP of G-SPANI-LDH-epoxy coating was −0.200 V, which was higher than that of pure-epoxy (-0.565 V) and G-epoxy coating (-0.446 V). This evidence indicates that G-SPANI-LDH-epoxy coating can be applied to long-term anticorrosion.

EIS can show the barrier effect of the coating more intuitively. As displayed in Fig. 4a1-4c2, during the initial soaked stage, the coatings were complete and defect free, and there was no water penetration. Low frequency impedance shows that G-SPANI-LDH-epoxy coating has the highest impedance modulus, while pure-epoxy coating has the lowest impedance modulus. With the prolongation of immersion time, the barrier effect of pure-epoxy coating is gradually weakened. When pure-epoxy coating was soaked for 70 days, the second time constant of epoxy coating appeared gradually, which indicated that water and chloride ions had already penetrated into the interface between coating and metal. The equivalent circuit changed from Fig. 4g1 to Fig. 4g2, water seepage occurred in the epoxy coating and emerged charge transfer resistance (R_{ct}) and electric double-layer capacitance (Q_{dl}), and the

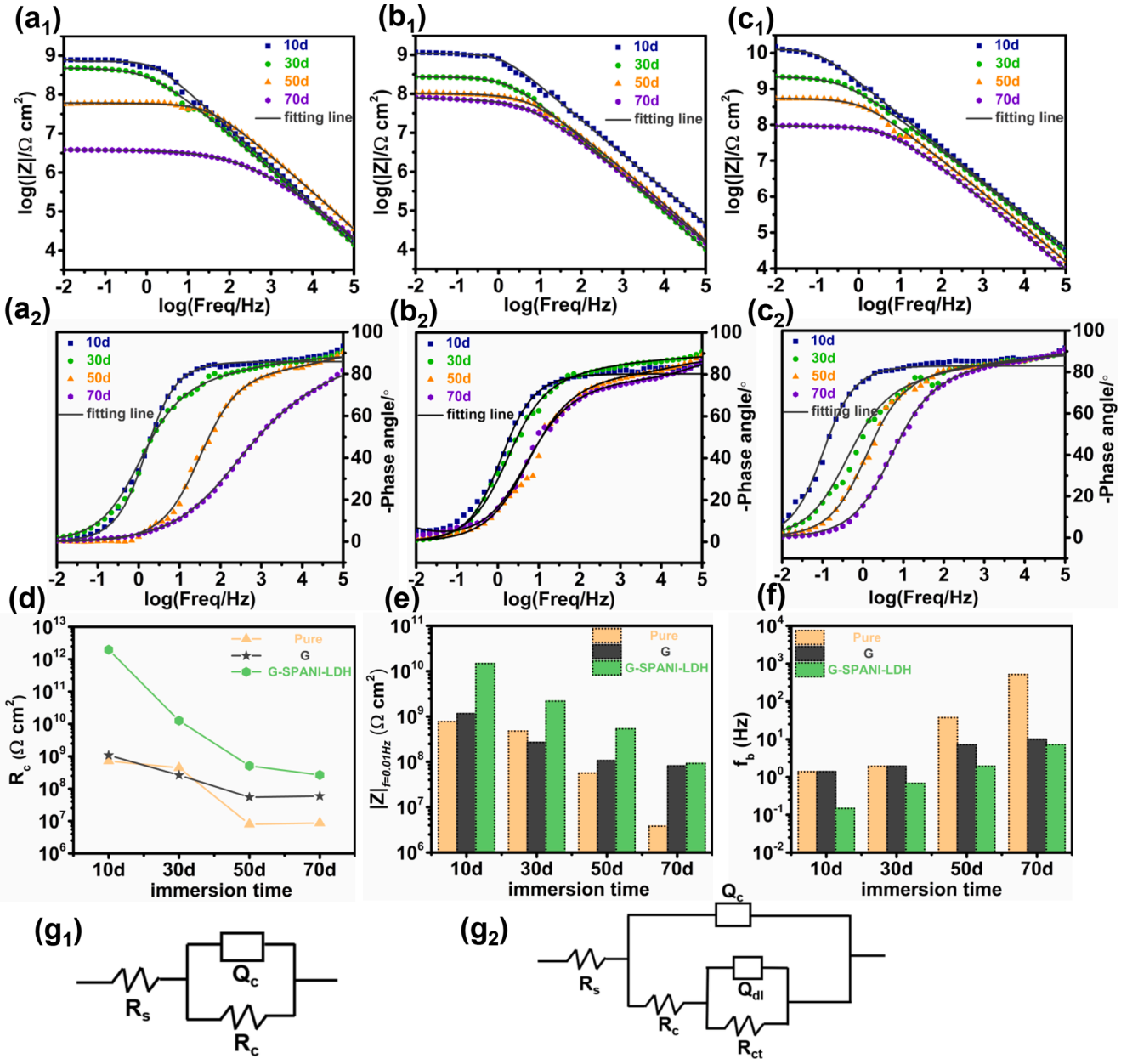

Fig. 4. Bode plots of a_1, a_2) pure-epoxy coating, b_1, b_2) G-epoxy coating, c_1, c_2) G-SPANI-LDH-epoxy coating. d) coating resistance over time, e) initial impedance ($|Z|_{f=0.01Hz}$) and f) breakpoint frequency (f_b) of different samples with time. The equivalent circuits (model g_1, g_2) are used to fit the EIS results of the coatings.

resistance of pure-epoxy coating decreased from 7.176 × 10^8 Ω cm^2 (10 d) to 8.679 × 10^6 Ω cm^2 (70 d).

For G-epoxy coating, the barrier performance is better than pure-epoxy coating, but the impedance of G-epoxy coating was even lower than pure-epoxy coating at 30 days. Because graphene is not dispersed totally in the epoxy resin, the aggregation phenomena and barrier shielding effect of graphene compete with each other, which influence the anticorrosion properties of the coating.

For G-SPANI-LDH-epoxy coating, a large number of hydroxyl groups on the surface of LDH improved the interface combination between G-SPANI-LDH and epoxy (the cross-section morphology of the coating also confirmed this point). The coating has not been observed water seepage in long-term service. Both G-epoxy coating and G-SPANI-LDH-epoxy coating have not appeared one new relaxation time, which indicated their excellent barrier properties and good intactness on the steel substrate. The equivalent circuit of G-epoxy coating and G-SPANI-LDH-epoxy coating is shown in Fig. 4g1.

The coating resistances were obtained from the equivalent circuits, which could express the barrier effect of the coating roughly. As shown in Fig. 4d, the resistance of G-SPANI-LDH-epoxy coating was always higher than that of pure-epoxy and G-epoxy coatings. However, the resistance of G-epoxy was lower than pure-epoxy at 30 days, which is consistent with OCP. Due to the agglomeration of graphene, the resistance of G-epoxy coating was reduced. With the extension of immersion time, the barrier performance of graphene gradually takes the upper hand, and the OCP and coating resistances of G-epoxy coating are gradually higher than that of pure-epoxy coating. Fig. 4e shows the impedance changes with time at 0.01 Hz for the three different coatings. The impedances at 0.01Hz are positively correlated with the barrier performance of the coatings, and the G-SPANI-LDH-epoxy coating always keeps the highest impedance. The breakpoint frequency (f_b) is the frequency at -45 phase angle, which can be obtained from the Bode diagram to evaluate the protective performances of the coatings [49–51]. The breakpoint frequency (f_b) is positively correlated with the delamination of the coating. The breakpoint frequencies of the three coatings are shown in Fig. 4f. With the prolongation of immersion time, pure-epoxy coating has the highest breakpoint frequency, indicating the delamination phenomenon is most serious. However, the G-SPANI-LDH-epoxy coating has the lowest breakpoint frequency, which are primarily ascribed to two points. On the one hand, G-SPANI-LDH can prevent the penetration of corrosive medium; on the other hand, it can accelerate the formation of passive film, prevent the diffusion of electrolyte to the coating/metal interface, and effectively delay the delamination of coating.

The polarization curves of the samples with thickness of 19 ± 1 μm after soaking for 15 days are measured in Fig. 5. According to the formula $v_{corr}=\frac{Ai_{corr}}{n\rho F}$, (A is the molar mass of Fe, i_{corr} is the corrosion current during polarization, the chemical valence (n) of Fe is 2, the density (ρ) of Q235 is 7.85 g/cm^3, and F is the Faraday constant (F = 96485 C/mol)). As shown in Table 2, the E_{corr} of epoxy is -596 mV, which is more positive than the E_{corr} of Q235 (-745 mV). Moreover, the higher E_{corr} (-574 mV for G-epoxy and -531 mV for G-SPANI-LDH-epoxy) indicates that nanofillers can provide better barrier performance. Corrosion current is positively correlated with corrosion rate. The G-SPANI-LDH-epoxy has the lowest corrosion current (4.921 × 10^{-8} A/cm^2), while the i_{corr} of pure-epoxy is 5.527 × 10^{-6} A/cm^2. The corrosion rate of the sample can be calculated by the following formula: $v_{corr(Q235)} \gg v_{corr(EP)} > v_{corr(G/EP)} \gg v_{corr(G\text{-}SPANI\text{-}LDH/EP)}$.The inhibition efficiency is calculated by the following formula: $IE=\frac{i_{corr}^{bare}-i_{corr}}{i_{corr}^{bare}} \times 100\%$, the corrosion inhibition efficiency of G-SPANI-LDH-epoxy coating is the highest.

3.5. Self-healing performance and salt spray resistance of scratch coating

To investigate the protection mechanism of G-SPANI-LDH hybrids, the artificial scratches were made on the surfaces of the composite coatings and the self-healing performance was evaluated by LEIS technique. The defective coatings were immersed in 3.5 wt% NaCl solution for 30 h and tested at 1, 15 and 30 h. As shown in Fig. 6a1-6c3, all the coatings are presenting low in the middle and high on the both sides, which demonstrating that the resistances of scratch areas are lower than the intact parts. For pure-epoxy and G-epoxy coatings, due to lack of coating protection, the scratches are corroded at the beginning of immersion.

As the soaking time increases, the scratches of pure-epoxy and G-epoxy coatings are severe corroded. Meanwhile, oxygen, water and chloride ions can permeate into the coatings through the scratches, so the resistances of the coatings are decreased synchronously. Because of lacking nanofillers in the pure-epoxy coating, the resistance of pure-epoxy coating is lowest after being soaked for 30 h.

For G-SPANI-LDH-epoxy coating, the resistance of scratch is higher than that in G-epoxy and pure-epoxy coatings. This phenomenon is mainly owing to the passivation of scratched area by SPANI nanoparticles to form an oxide layer which decreases the local electrochemical activity of the steel. In horizontal comparison of Fig. 6c1, Fig. 6c2 and Fig. 6c3, we find the corrosion is slowly happening and the whole resistance of the G-SPANI-LDH-epoxy coating is gradually decreasing. In vertical comparison of Fig. 6(a1-a3), Fig. 6(b1-b3) and Fig. 6(c1-c3), the corrosion condition of G-SPANI-LDH-epoxy coating is least. These phenomena indicate that the passive film can slow down the corrosion process by reducing regional electrochemical activity.

Fig. 6d and Fig. 6e show the average resistances and minimum resistances, the average resistances describe the average resistances of thescratched area and the intact area near the scratch and the minimum resistances represent the minimum resistances of the scratched area. As shown in Fig. 6d, the average resistances of G-SPANI-LDH-epoxy coating always keep the highest, which are consistent with the LEIS mappings. In Fig. 6e, the minimum resistance of G-SPANI-LDH-epoxy coating is higher than that in pure-epoxy and G-epoxy coatings after 30 h

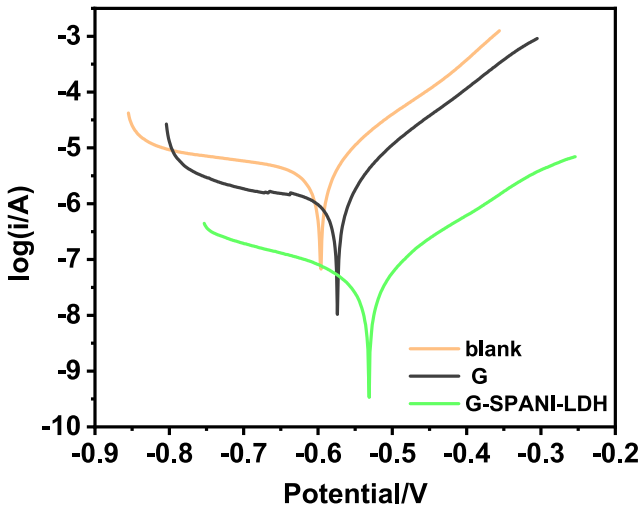

Fig. 5. The polarization curves of pure-epoxy coating, G-epoxy coating and G-SPANI-LDH-epoxy coating.

Table 2
Electrochemical parameters of Q235 electrodes without and with coatings immersed in 3.5 wt% NaCl solution.

Sample	E_{corr}vs SCE mV	i_{corr} A/cm^2	v_{corr} mm/year	IE/%
Bare Q235[5]	−745	7.455 × 10^{-5}	0.869	\
Pure-epoxy	−596	5.527 × 10^{-6}	6.443 × 10^{-2}	92.586
G-epoxy	−574	1.956 × 10^{-6}	2.280 × 10^{-2}	97.376
G-SPANI-LDH-epoxy	−531	4.921 × 10^{-8}	5.737 × 10^{-4}	99.934

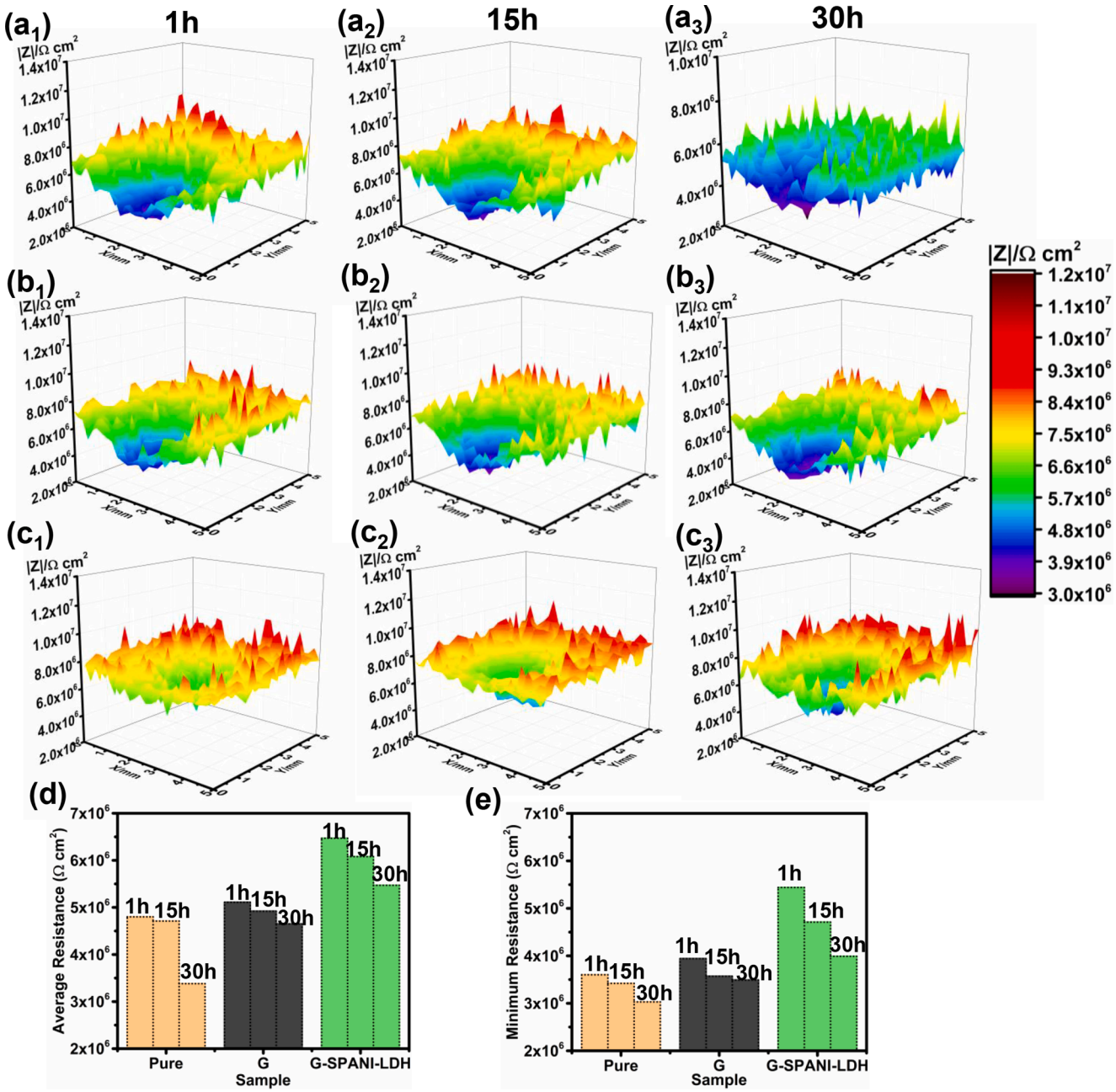

Fig. 6. The LEIS mappings of a_1, a_2, a_3) pure-epoxy, b_1, b_2, b_3) G-epoxy and c_1, c_2, c_3) G-SPANI-LDH-epoxy. d) The average resistance of scratched sample and e) minimum resistance of scratched area as a function of immersion time.

immersion, which revealing the passivation film can delay corrosion.

As shown in Fig. 7, pure-epoxy coating was corroded rapidly at the defect in the atmosphere of high salt and high humidity. A large number of corrosive media got into coatings along the defects, causing the coating bubble, interface delamination and coating failure after 250 h. Compared with the pure-epoxy coating, it was found that the corrosive conditions of G-epoxy coating and G-SPANI-LDH-epoxy coating were not obvious, especially G-SPANI-LDH-epoxy coating was more prominent.

3.6. Analysis of corrosion products

After 70 days immersion in 3.5 wt% NaCl solution, the coatings covered on the steels were removed and the substrates were cleaned by ethanol three times to eliminate the contaminants. The surface morphologies of substrates were characterized by SEM, the compositions and distributions of corrosion products were analyzed by Raman spectroscopy. As shown in Fig. 8a, the surface of pure-epoxy coating becomes uneven and appears corrosion pits. The surface of severe corroded steel is mainly composed of Fe, O and C elements. For G-epoxy coating, the surface of steel becomes smooth, indicating the high impermeability of graphene can prevent oxygen infiltration. Surprisingly, the surface of G-SPANI-LDH-epoxy coating become glossier and the proportion of Fe and O is the highest. It might be attributed to the outstanding dispersion of graphene and the passivation of conductive polymer SPANI.

In order to further analyze the corrosion phenomena, we characterized the corrosion products. As shown in Fig. 8b, the corrosion products of pure-epoxy coating are made up of α-FeOOH (396 cm^{-1}),

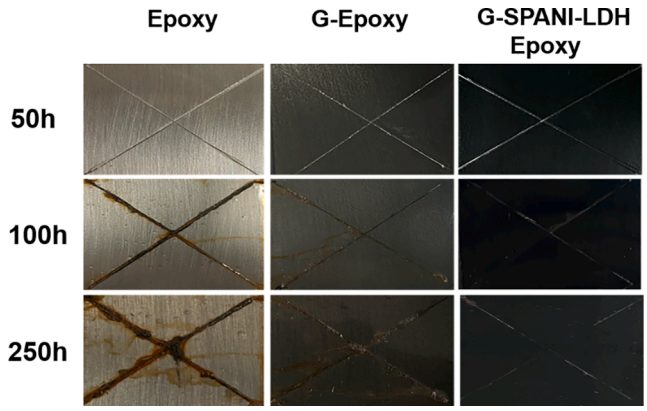

Fig. 7. The salt spray test of scratch coatings.

γ-FeOOH (1300 cm^{-1}), Fe_2O_3 (285 cm^{-1}) and Fe_3O_4 (545 cm^{-1}, 668 cm^{-1}) [52]. For G-epoxy coating, the contents of α-FeOOH (396 cm^{-1}) and γ-FeOOH (1300 cm^{-1}) are gradually decreased, and the content of Fe_2O_3 (285 cm^{-1}) is improved. Furthermore, the peaks of α-FeOOH (396 cm^{-1}), γ-FeOOH (1300 cm^{-1}) are nearly disappearing in G-SPANI-LDH-epoxy, the contents of Fe_2O_3 (285 cm^{-1}) and Fe_3O_4 (545 cm^{-1}, 668 cm^{-1}) are significantly increased, which indicating that graphene can prevent oxygen from permeating and doped conductive polymers oxidize iron to form Fe_2O_3 and Fe_3O_4.

The distributions of corrosion products in the pure-epoxy, G-epoxy and G-SPANI-LDH-epoxy coatings are described by Raman mapping in Fig. 8c. For pure-epoxy coating, the α-FeOOH is intently distributed on the substrate, and the Fe_2O_3 and Fe_3O_4 are like "isolated island" interspersed on the steel. The "islands" of Fe_2O_3 and Fe_3O_4 are enlarged and the content of α-FeOOH is lower in the G-epoxy coating. For G-SPANI-LDH-epoxy coating, the Fe_2O_3 and Fe_3O_4 are distributed over the entire surface, the α-FeOOH is only existed sporadically.

3.7. Protection mechanism of coating

As shown in Fig. 9, the protective mechanism of G-SPANI-LDH-epoxy coating is split into two periods: in the beginning of immersion, the intact coating acts as a "protective cover" to prevent external substances from

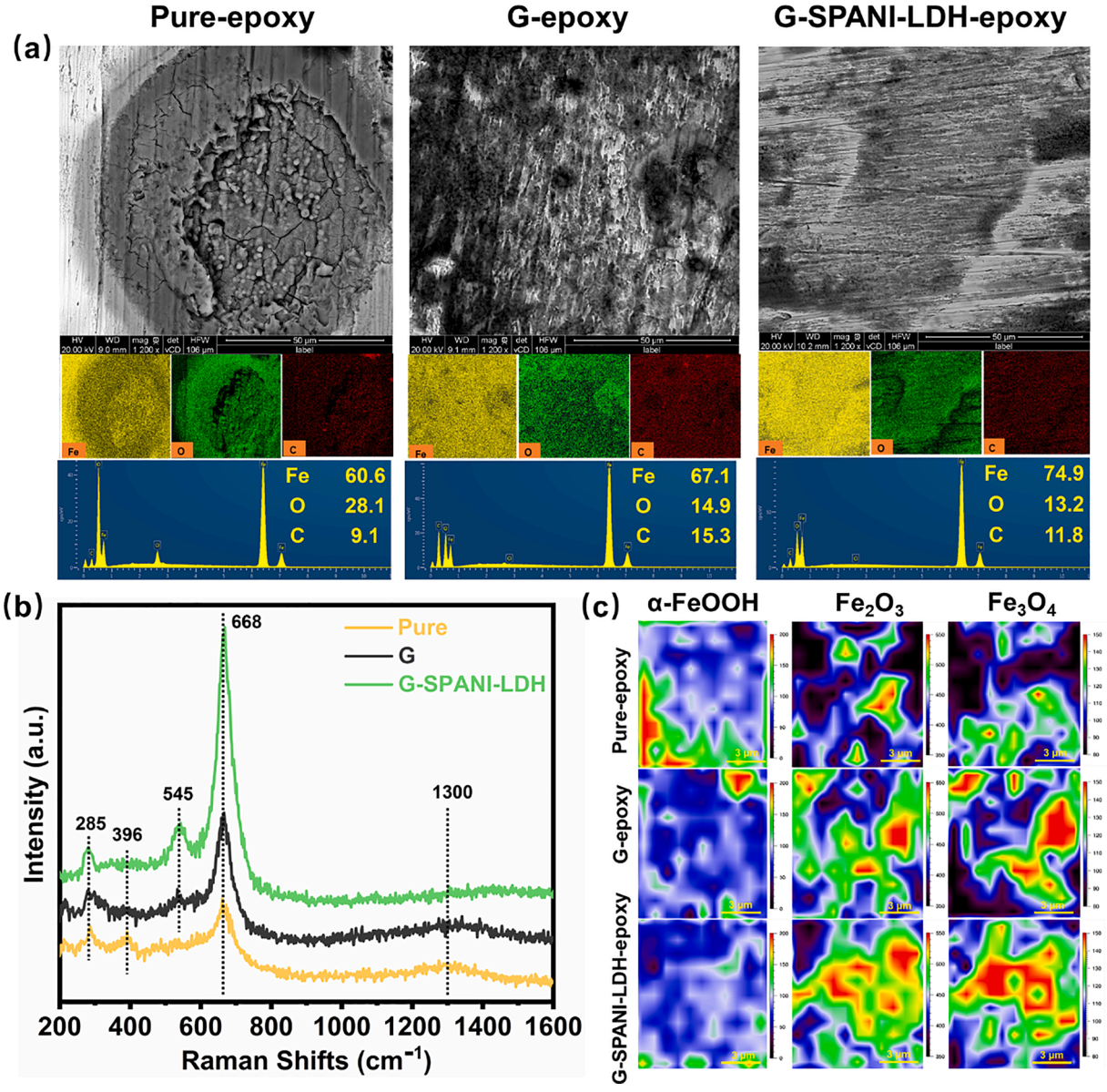

Fig. 8. a) The SEM and EDS of corrosion product, b) the Raman spectra of corrosion product, c) the Raman mappings of corrosion product.

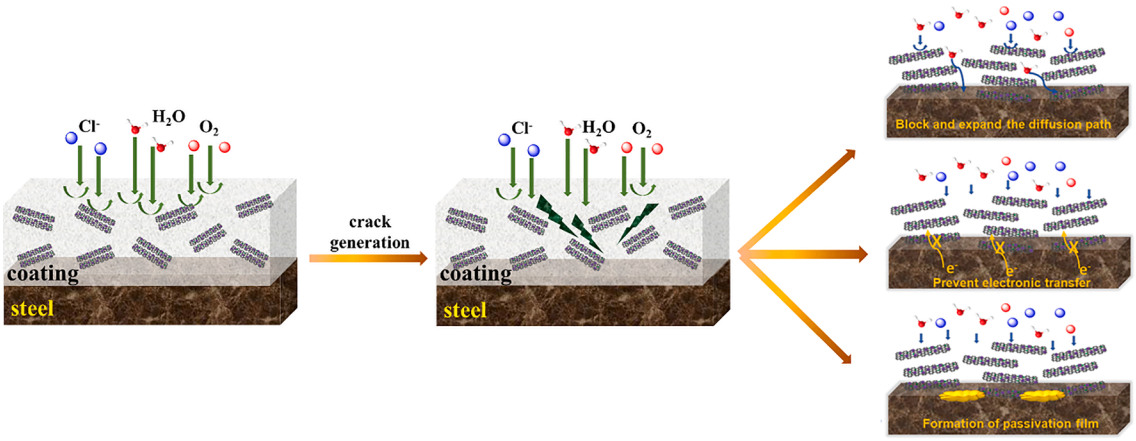

Fig. 9. The protection mechanism of G-SPANI-LDH-epoxy coating.

contacting the metal substrate. Once the organic coating is immersed in salt water for a long time, chloride ions, water and oxygen will penetrate into the coating, which will easily lead to microcracks and micropores. At this time, the modified filler G-SPANI-LDH mainly plays a triple role: 1. The unprecedented barrier property of graphene can extend the diffusion path, and LDH on the surface can improve the compatibility between the composite and resin. 2. Galvanic corrosion consists of four elements: cathode, anode, electrolyte and conductor. When one of these links disappears, corrosion stops immediately. The surface insulation can prevent charge transfer and avoid the formation of conductive path, galvanic corrosion would not occur. 3. Conducting polymer passivates the substrate. Sulfonated polyaniline, as a conductive polymer, can accept the electrons released by metal dissolution and reduce it from oxidation state (doped form) to reduced state (undoped form), and the increasing iron ions (Fe^{2+} and Fe^{3+}) change into passive Fe_2O_3 and Fe_3O_4 oxide layers [22,53]. The corrosion resistance of the composite coating was improved by the synergistic action of the three elements.

4. Conclusion

In summary, we report an environmentally friendly water-based epoxy coating which combines the sulfonated polyaniline-functionalized graphene sheet with LDH insulation package. TEM, SEM, XRD, Raman and XPS analysis confirmed the successful encapsulation of graphene nanosheets by LDH. Compared with the conductivity of original graphene, the surface coated LDH can effectively reduce the conductivity of graphene, and also significantly improves the interfacial compatibility between the material and the resin. The long-term electrochemical results show that the corrosion resistance of G-SPANI-LDH-epoxy is obviously improved compared with pure-epoxy and G-epoxy without SPANI and LDH, which is attributed to the enhanced barrier property of G-SPANI-LDH-epoxy, the strong interface bonding between G-SPANI-LDH and epoxy matrix, and the passivation effect of interlayer SPANI. In addition, through the surface morphology and distribution of corrosion products, it can be found that the metal substrate under pure epoxy coating is seriously corroded due to the penetration of corrosion medium; while the sample with G-SPANI-LDH filler increases the content of ferric oxide, and dense oxide films formed on the surface can protect the metal from corrosion. In short, this novel sulfonated polyaniline assisted hierarchical assembly of graphene-LDH nanohybrid based epoxy coating combines the reduced conductivity of graphene, the improved affinity between the fillers and resin, with the realization of self-healing performance in anticorrosive coatings.

Declaration of Competing Interest

The authors declare that they have no known competing financial interests or personal relationships that could have appeared to influence the work reported in this paper.

Acknowledgments

The authors gratefully thank the financial support provided by the “One Hundred Talented People” of the Chinese Academy of Sciences (No. Y60707WR04); the Key Research Program of Frontier Sciences of the Chinese Academy of Sciences (No. QYZDY-SSW-JSC009) and K.C. Wong Education Foundation (GJTD-2019-13).

Appendix A. Supplementary data

Supplementary data to this article can be found online at https://doi.org/10.1016/j.cej.2021.131269.

References

[1] J. Lei, Y. Hu, Z. Liu, G.J. Cheng, K. Zhao, Defects Mediated Corrosion in Graphene Coating Layer, ACS Appl. Mater. Interfaces 9 (13) (2017) 11902–11908, https://doi.org/10.1021/acsami.7b01539.
[2] M. Zhu, Z. Du, Z. Yin, W. Zhou, Z. Liu, S.H. Tsang, E.H.T. Teo, Low-Temperature in Situ Growth of Graphene on Metallic Substrates and Its Application in Anticorrosion, ACS Appl. Mater. Interfaces 8 (1) (2016) 502–510, https://doi.org/10.1021/acsami.5b0945310.1021/acsami.5b09453.s001.
[3] X. Luo, S. Yuan, X. Pan, C. Zhang, S. Du, Y. Liu, Synthesis and Enhanced Corrosion Protection Performance of Reduced Graphene Oxide Nanosheet/ZnAl Layered Double Hydroxide Composite Films by Hydrothermal Continuous Flow Method, ACS Appl. Mater. Interfaces 9 (21) (2017) 18263–18275, https://doi.org/10.1021/acsami.7b0258010.1021/acsami.7b02580.s001.
[4] V.M. Stanković, I. Jevremović, I. Jung, K. Rhee, Electrochemical study of corrosion behavior of graphene coatings on copper and aluminum in a chloride solution, Carbon 75 (2014) 335–344, https://doi.org/10.1016/j.carbon.2014.04.012.
[5] S. Qiu, W. Li, W. Zheng, H. Zhao, L. Wang, Synergistic Effect of Polypyrrole-Intercalated Graphene for Enhanced Corrosion Protection of Aqueous Coating in 3.5% NaCl Solution, ACS Appl. Mater. Interfaces 9 9 (39) (2017) 34294–34304, https://doi.org/10.1021/acsami.7b0832510.1021/acsami.7b08325.s001.
[6] Y.N. Singhbabu, B. Sivakumar, J.K. Singh, H. Bapari, A.K. Pramanick, R.K. Sahu, Efficient anti-corrosive coating of cold-rolled steel in a seawater environment using an oil-based graphene oxide ink, Nanoscale 7 (17) (2015) 8035–8047, https://doi.org/10.1039/C5NR01453K.
[7] H. Lu, S. Zhang, W. Li, Y. Cui, T. Yang, Synthesis of Graphene Oxide-Based Sulfonated Oligoanilines Coatings for Synergistically Enhanced Corrosion Protection in 3.5% NaCl Solution, ACS Appl. Mater. Interfaces 9 9 (4) (2017) 4034–4043, https://doi.org/10.1021/acsami.6b13722.
[8] B. Ramezanzadeh, A. Ahmadi, M. Mahdavian, Enhancement of the corrosion protection performance and cathodic delamination resistance of epoxy coating through treatment of steel substrate by a novel nanometric sol-gel based silane composite film filled with functionalized graphene oxide nanosheets, Corros. Sci. 109 (2016) 182–205, https://doi.org/10.1016/j.corsci.2016.04.004.

[9] M. Fang, Z. Zhang, J. Li, H. Zhang, H. Lu, Y. Yang, Constructing hierarchically structured interphases for strong and tough epoxy nanocomposites by amine-rich graphene surfaces, J. Mater. Chem. 20 (2010) 9635–9643, https://doi.org/10.1039/c0jm01620a.

[10] J. Ma, Q. Meng, A. Michelmore, N. Kawashima, Z. Izzuddin, C. Bengtsson, H. Kuan, Covalently bonded interfaces for polymer/graphene composites, J. Mater. Chem. A 13 (2013) 4255–4264, https://doi.org/10.1039/c3ta01277h.

[11] B. Ramezanzadeh, G. Bahlakeh, M. Ramezanzadeh, Polyaniline-cerium oxide (PAni-CeO_2) coated graphene oxide for enhancement of epoxy coating corrosion protection performance on mild steel Check, Corros. Sci. 137 (2018) 111–126, https://doi.org/10.1016/j.corsci.2018.03.038.

[12] T. Umeyama, J. Baek, J. Mihara, N.V. Tkachenko, H. Imahori, Occurrence of photoinduced charge separation by the modulation of the electronic coupling between pyrene dimers and chemically converted graphenes, Chem. Commun. 53 (6) (2017) 1025–1028, https://doi.org/10.1039/C6CC07985G.

[13] M. Varenik, M.J. Green, O. Regev, Distinguishing Self-Assembled Pyrene Structures from Exfoliated Graphene, Langmuir 32 (41) (2016) 10699–10704, https://doi.org/10.1021/acs.langmuir.6b0337910.1021/acs.langmuir.6b03379.s001.

[14] L. Li, X. Zheng, J. Wang, Q. Sun, Q. Xu, Solvent-Exfoliated and Functionalized Graphene with Assistance of Supercritical Carbon Dioxide, ACS Sustain. Chem. Eng. 1 (1) (2013) 144–151, https://doi.org/10.1021/sc3000724.

[15] A.Z. AlZahrani, First-principles study on the structural and electronic properties of graphene upon benzene and naphthalene adsorption, Appl. Surf. Sci. 257 (2010) 807–810, https://doi.org/10.1016/j.apsus.2010.07.069.

[16] P. Khanra, T. Kuila, S.H. Bae, N.H. Kim, J.H. Lee, Electrochemically exfoliated graphene using 9-anthracene carboxylic acid for supercapacitor application, J. Mater. Chem. 22 (46) (2012) 24403, https://doi.org/10.1039/c2jm34838a.

[17] E. Zarudnev, S. Stepanian, L. Adamowicz, V. Karachevtsev, Noncovalent Interaction of Graphene with Heterocyclic Compounds: Benzene, Imidazole, Tetracene, and Imidazophenazines, ChemPhysChem. 17 (8) (2016) 1204–1212, https://doi.org/10.1002/cphc.v17.810.1002/cphc.201500839.

[18] A. Ghosh, K.V. Rao, S. George, C.N.R. Rao, Noncovalent Functionalization, Exfoliation, and Solubilization of Graphene in Water by Employing a Fluorescent Coronene Carboxylate, Chem. Eur. J. 16 (9) (2010) 2700–2704, https://doi.org/10.1002/chem.200902828.

[19] E.G. Gordeev, M.V. Valentine, P. Ananikov, Fast and accurate computational modeling of adsorption on graphene: a dispersion interaction challenge, Phys. Chem. Chem. Phys. 15 (2013) 18815–18821, https://doi.org/10.1039/c3cp53189a.

[20] C. Chen, S.H. Qiu, M.J. Cui, S.L. Qin, G. Yan, H.C. Zhao, L.P. Wang, Q.J. Xue, Achieving high performance corrosion and wear resistant epoxy coatings via incorporation of noncovalent functionalized graphene, Carbon 114 (2017) 356–366, https://doi.org/10.1016/j.carbon.2016.12.044.

[21] S. Jo, Y.H. Park, S.G. Ha, S.M. Kim, C. Song, S.Y. Park, I. In, Simple noncovalent hybridization of polyaniline with graphene and its application for pseudocapacitor, Synth. Met. 209 (2015) 60–67, https://doi.org/10.1016/j.synthmet.2015.06.004.

[22] M. Cui, S. Ren, J. Pu, Y. Wang, H. Zhao, L. Wang, Poly(o-phenylenediamine) modified graphene toward the reinforcement in corrosion protection of epoxy coatings, Corros. Sci. 159 (2019) 108131, https://doi.org/10.1016/j.corsci.2019.108131.

[23] J. Zhang, J. Lei, R. Pan, Y. Xue, H. Ju, Highly sensitive electrocatalytic biosensing of hypoxanthine based on functionalization of graphene sheets with water-soluble conducting graft copolymer, Biosens. Bioelectron. 26 (2) (2010) 371–376, https://doi.org/10.1016/j.bios.2010.07.127.

[24] N. Maity, R. Ghosh, A.K. Nandi, Optoelectronic Properties of Self-Assembled Nanostructures of Polymer Functionalized Polythiophene and Graphene, Langmuir 34 (26) (2018) 7585–7597, https://doi.org/10.1021/acs.langmuir.7b04387.

[25] M.J. Cui, S.M. Ren, H.C. Zhao, Q.J. Xue, L.P. Wang, Polydopamine coated graphene oxide for anticorrosive reinforcement of water-borne epoxy coating, Chem. Eng. J. 335 (2018) 255–266, https://doi.org/10.1016/j.cej.2017.10.172.

[26] P. Du, J. Wang, G. Liu, H. Zhao, L. Wang, Facile synthesis of intelligent nanocomposites as encapsulation for materials protection, Mater. Chem. Front. 3 (2) (2019) 321–330, https://doi.org/10.1039/C8QM00455B.

[27] W. Sun, L. Wang, T. Wu, Y. Pan, G. Liu, Inhibited corrosion-promotion activity of graphene encapsulated in nanosized silicon oxide, J. Mater. Chem. A 3 (32) (2015) 16843–16848, https://doi.org/10.1039/C5TA04236D.

[28] W. Sun, L. Wang, T. Wu, Y. Pan, G.C. Liu, Synthesis of low-electrical-conductivity graphene/per-nigraniline composites and their application in corrosion protection, Carbon 79 (2014) 605–614, https://doi.org/10.1016/j.carbon.2014.08.021.

[29] W. Sun, L. Wang, T. Wu, M. Wang, Z. Yang, Y. Pan, G. Liu, Inhibiting the Corrosion-Promotion Activity of Graphene, Chem. Mat. 27 (7) (2015) 2367–2373, https://doi.org/10.1021/cm5043099.

[30] J. Ding, H. Zhao, Y. Zheng, X. Zhao, H. Yu, A long-term anticorrsive coating through graphene passivation, Carbon 138 (2018) 197–206, https://doi.org/10.1016/j.carbon.2018.06.018.

[31] Z. Yang, W. Sun, L. Wang, S. Li, T. Zhu, G. Liu, Liquid-phase exfoliated fluorographene as a two-dimensional coating filler for enhanced corrosion protection performance, Corros. Sci. 103 (2016) 312–318, https://doi.org/10.1016/j.corsci.2015.10.039.

[32] J. Ding, H. Zhao, D. Ji, B. Xu, X. Zhao, Z. Wang, D. Wang, Q. Zhou, H. Yu, Achieving long-term anticorrosion via the inhibition of graphene's electrical activity, J. Mater. Chem. A 7 (6) (2019) 2864–2874, https://doi.org/10.1039/C8TA10337B.

[33] H.L. Poh, P. Šimek, Z. Sofer, M. Pumera, Halogenation of graphene with chlorine, bromine, or iodine by exfoliation in a halogen atmosphere, Chemistry 19 (8) (2013) 2655–2662, https://doi.org/10.1002/chem.201202972.

[34] R. Lee, C. Chi, Y. Hsu, Platinum nanoparticle/self-doping polyaniline composite-based counter electrodes for dye-sensitized solar cells, J. Nano. Res. 15 (2013) 1733, https://doi.org/10.1007/s11051-013-1733-z.

[35] L.u. Shi, F. Zeng, X. Cheng, K.H. Lam, W. Wang, A. Wang, Z. Jin, F. Wu, Y. Yang, Enhanced performance of lithium-sulfur batteries with high sulfur loading utilizing ion selective MWCNT/SPANI modified separator, Chem. Eng. J. 334 (2018) 305–312, https://doi.org/10.1016/j.cej.2017.08.015.

[36] Y. Fu, Q. Sheng, J. Zheng, The novel sulfonated polyaniline-decorated carbon nanosphere nanocomposites for electrochemical sensing of dopamine, New J. Chem. 41 (24) (2017) 15439–15446, https://doi.org/10.1039/C7NJ03086J.

[37] S.H. Qiu, C. Chen, W.R. Zheng, W. Li, H.C. Zhao, L.P. Wang, Long-term corrosion protection of mild steel by epoxy coating containing self-doped polyaniline nanofiber, Synth. Met. 229 (2017) 39–46, https://doi.org/10.1016/j.synthmet.2017.05.004.

[38] M. Aymen, S. Sami, S. Ahmed, G. Fethi, B. Abdellatif, Correlation between Raman spectroscopy and electrical conductivity of graphite/polyaniline composites reacted with hydrogen peroxide, J. Phys. D: Appl. Phys. 46 (2013), 335103, https://doi.org/10.1088/0022-3727/46/33/335103.

[39] A. Shakoor, T. Rizvi, Raman spectroscopy of conducting poly (methyl methacrylate)/polyaniline dodecylbenzenesulfonate blends, J. Raman Spectrosc. 41 (2010) 237–240, https://doi.org/10.1002/jrs.2414.

[40] B. Roy, M. Gupta, L. Bhowmik, J. Ray, Studies on water soluble conducting polymer-aniline initiated polymerization of m-aminobenzene sulfonic acid, Synth. Met. 100 (1999) 233–236. https://doi.org./10.1016/S0379-6779(98)01505-7.

[41] M. Trchova, Z. Moravkova, M. Blaha, J. Stejskal, Raman spectroscopy of polyaniline and oligoaniline thin films, Electrochim. Acta 122 (2014) 28–38. http://doi.org./10.1016/j.electacta.2013.10.133.

[42] Y. Su, S.H. Qiu, D.P. Yang, S. Liu, H.C. Zhao, L.P. Wang, Q.J. Xue, Active anti-corrosion of epoxy coating by nitrite ions intercalated MgAl LDH, J. Hazard. Mater. 391 (2020), 122215, https://doi.org/10.1016/j.jhazmat.2020.122215.

[43] S. Zhang, Understanding of Sulfurized Polyacrylonitrile for Superior Performance Lithium/Sulfur Battery, Energies 7 (2014) 4588–4600, https://doi.org/10.3390/en7074588.

[44] J. Yan, B. Li, X. Liu, Nano-porous sulfur–polyaniline electrodes for lithium sulfur-batteries, Nano Energy 18 (2015) 245–252, https://doi.org/10.1016/j.nanoen.2015.10.024.

[45] M.J. Cui, S.M. Ren, S.L. Qin, Q.J. Xue, H.C. Zhao, L.P. Wang, Processable poly(2-butylaniline)/heXagonal boron nitride nanohybrids for synergetic anticorrosive reinforcement of epoxy coating, Corros. Sci. 131 (2018) 187–198, https://doi.org/10.1016/j.corsci.2017.11.022.

[46] C.B. Liu, H.C. Zhao, P. Hou, B. Qian, X. Wang, C. Guo, L.P. Wang, Efficient Graphene/Cyclodextrin-Based nanocontainer: synthesis and host-guest inclusion for self-healing anticorrosion application, ACS Appl. Mater. Interfaces 42 (2018) 36229–36239, https://doi.org/10.1021/acsami.8b11108.

[47] X. Luo, J. Zhong, Q. Zhou, S. Du, S. Yuan, Y. Liu, Cationic reduced graphene oxide as self-aligned nanofiller in the epoxy nanocomposite coating with excellent anticorrosive performance and its high antibacterial activity, ACS Appl. Mater. Interfaces 10 (21) (2018) 18400–18415, https://doi.org/10.1021/acsami.8b0198210.1021/acsami.8b01982.s001.

[48] S.H. Qiu, Y. Su, H.C. Zhao, L.P. Wang, Q.J. Xu, Ultrathin metal-organic framework nanosheets prepared via surfactant-assisted method and exhibition of enhanced anticorrosion for composite coatings, Corros. Sci. 178 (2021), 109090, https://doi.org/10.1016/j.corsci.2020.109090.

[49] E. Potvin, L. Brossard, G. Larochelle, Corrosion protective performances of commercial low-VOC epoxy/urethane coatings on hot-rolled 1010 mild steel, Prog. Org. Coat. 31 (4) (1997) 363–373, https://doi.org/10.1016/S0300-9440(97)00095-7.

[50] B. Ramezanzadeh, E. Ghasemi, M. Mahdavian, E. Changizi, M.H. Mohamadzadeh Moghadam, Moghadam Covalently-grafted graphene oxide nanosheets to improve barrier and corrosion protection properties of polyurethane coatings, Carbon 93 (2015) 555–573, https://doi.org/10.1016/j.carbon.2015.05.094.

[51] B. Ramezanzadeh, S. Niroumandrad, A. Ahmadi, M. Mahdavian, M.H.M. Moghadam, Enhancement of barrier and corrosion protection performance of an epoxy coating through wet transfer of amino functionalized graphene oxide, Corros. Sci. 103 (2016) 283–304. https://doi.org.10.1016/j.corsci.2015.11.033.

[52] Y. Ye, D. Zhang, Z. Liu, W. Liu, H. Zhao, L. Wang, X. Li, Anti-corrosion properties of oligoaniline modified silica hybrid coatings for low-carbon steel, Synth. Met. 235 (2018) 61–70, https://doi.org/10.1016/j.synthmet.2017.11.015.

[53] P. Kinlen, Y. Ding, D. Silverman, Corrosion Protection of Mild Steel Using Sulfonic and Phosphonic Acid-doped Polyanilines, Corrosion 58 (2002) 490−497. 0.5006/1.3277639.